




Solid surface frustrated Lewis pair constructed on layered AlOOH for hydrogenation reaction

Shulin Liu^{1,2,3}, Minghua Dong^{1,2,3}, Yuxuan Wu^{1,2}, Sen Luan^{1,2}, Yu Xin^{1,2}, Juan Du^{1,2}, Shaopeng Li^{1,2}, Huizhen Liu^{1,2}   & Buxing Han^{1,2} 

Designing heterogeneous solid surface frustrated Lewis pair (ssFLP) catalyst for hydrogenation is a new challenge in catalysis and no research has been reported on the construction of ssFLP on boehmite (AlOOH) surfaces up to now as far as we know. Herein, AlOOH with a layer structure is prepared and it is found that the Lewis basic O_{H_v} site (one H removed from OH) and an adjacent Lewis acidic unsaturated Al site ($Al^{3+}_{unsatur}$) proximal to a surface OH_v (OH vacancy) on AlOOH layers could form the ssFLP. The layered structure of AlOOH and its abundant OH defects over the surface result in a high concentration of $O_{H_v}/Al^{3+}_{unsatur}$ FLPs, which are conducive to highly efficient hydrogen activation for hydrogenation of olefins and alkynes with low H-H bond dissociates activation energy of 0.16 eV under mild conditions ($T = 80^\circ C$ and $P(H_2) = 2.0$ MPa). This work develops a new kind of hydrogenation catalyst and provides a new perspective for creating solid surface FLP.

¹Beijing National Laboratory for Molecular Sciences, CAS Key Laboratory of Colloid and Interface and Thermodynamics, Institute of Chemistry, Chinese Academy of Sciences, Beijing 100190, China. ²School of Chemistry and Chemical Engineering, University of Chinese Academy of Sciences, Beijing 100049, China. ³These authors contributed equally: Shulin Liu, Minghua Dong. ✉email: liuhz@iccas.ac.cn

Hydrogen activation is the key step in catalytic hydrogenation reaction, which is very important in the petrochemical industry. The process has been well developed over transition metal complexes, metal-based heterogeneous catalysts¹ and nonmetallic N, S, B, or P heteroatom doped carbon-based catalyst^{2–6}. In 2006, W. Stephan group⁷ firstly reported a novel mode for H₂ activation that the frustrated Lewis pair (FLP) could activate H₂ and an appropriate distance between Lewis acid and base sites is critical⁸. The early research of FLP was based on molecular-based homogeneous complex^{9–12}, such as phosphide–boranes, which suffers the difficulties in catalyst recovery and product purification. Therefore, it is more expected to develop heterogeneous catalysts with FLP-like activity^{13,14}. The construction of surface FLP over noble-metal-based heterogeneous catalysts has been successfully demonstrated. For example, the formation of FLP consisting of sodium hydride (Na⁺H⁻) and a framework-bound hydroxy proton O(H⁺) is reported upon H₂ treatment of zeolite NaY loaded with Pt nanoparticles (Pt_x/NaY)¹⁵. The Au powders and molecular Lewis bases (for example, imine and nitrile) also could form FLP¹⁶.

It is well known that it is easy to construct defects on reducible oxides, beneficial from oxygen vacancies. Recently, solid surface FLP sites on reducible metal oxide CeO₂ were developed by Qu et al.¹⁷ since its reversible Ce³⁺/Ce⁴⁺ redox pair and rich surface defects chemistry. It was found that the richness of surface defects is the key to the construction of surface Lewis acidic center by two adjacent reduced surface Ce atoms near an oxygen vacancy and the neighboring surface lattice oxygen was Lewis base. Ozin and co-workers^{18–21} developed the surface FLP sites over In₂O_{3-x}(OH)_y composed of a Lewis basic surface OH adjacent to a Lewis acid indium proximal to an oxygen vacancy, which assisted the adsorption and heterolytic dissociation of H₂ in the reverse water gas shift (RWGS) reaction in photocatalysis. Ni-O Lewis pair at the NiO_x-Ni interface was also fabricated for the activation of water²². Obviously, the rational design and controllable construction of specific Lewis pairs with high catalytic performance are now limited to a few specific oxide systems through the formation of surface oxygen vacancies or construction of hydroxyl-metal ion pairs. The development of novel ssFLPs is very interesting from both scientific and practical perspectives and yet it is still a great challenge to construct an efficient ssFLPs site on inert metal oxide for hydrogenation reaction.

Boehmite (AlOOH), as one of the main components of bauxite ore, is abundant in natural resources²³ and has been studied extensively for various applications^{24–28}, such as adsorbents, porous materials, catalyst support. Especially, AlOOH is a main-group metal hydroxide and non-reducible. Herein, we prepared a series of layered AlOOH, where a novel ssFLPs site was found. With these layered AlOOH, the hydrogenation of olefins and alkynes could proceed efficiently under mild conditions (T = 80°C and P(H₂) = 2.0 MPa). It was found that the abundant OH vacancies (OH_v) are the key to the construction of the Lewis acid center. The ssFLPs were created by a Lewis basic O_{Hv} site and an adjacent Lewis acidic unsaturated Al site (Al³⁺_{unsatur.}) proximal to a surface OH vacancy on AlOOH layers. The unique layer structure of AlOOH and abundant OH defects result in a high concentration of O_{Hv} / Al³⁺_{unsatur.} FLPs, which are conducive to highly efficient hydrogen activation.

Results and discussion

Structural characterizations. The catalysts were prepared using Al(NO₃)₃·9H₂O as the precursor and urea as the precipitant by a solvothermal method at 180°C for 5 h, as shown in Fig. 1. When the mole ratio of urea and Al(NO₃)₃·9H₂O was 1:1, the catalyst was denoted as AlOx-U1. When the mole ratio of urea and

Al(NO₃)₃·9H₂O was above 1:1, the catalyst was denoted as AlOOH-Ux and x stands for the mole ratio of Al and urea used.

Transmission electron microscopy (TEM) images are shown in Fig. 2. AlOOH-U2, AlOOH-U3 and AlOOH-U4 presented layered structure, while AlOx-U1 showed the initial formation state of the layer due to the lower OH⁻ concentration from urea decomposition during the solvothermal reaction. Al and O elements were presented in the EDS mapping images with different colors, meaning successful acquisition of AlOOH. The catalysts were also characterized by powder X-ray diffraction (PXRD) and the results were shown in Fig. 3a. No peaks were observed in the PXRD pattern of AlOx-U1 due to the amorphous nature of AlOx made of a recipe of less urea. AlOOH-U2, AlOOH-U3 and AlOOH-U4 exhibited the typical peaks of orthorhombic AlOOH crystal structure²⁹ (JCPDS No. 21-1307), while the weak peak intensities indicated the poor crystallinity³⁰. The coexistence of small crystalline areas was shown in the following HR-TEM images (Fig. 2g), and several series of patterns, corresponding to (010) facets, can be found in FFT images. The (200), (002) and (10-1) facets which are orthogonal to the (010) facets can be observed in the images. It demonstrates that as-prepared AlOOH exposed (010) facets. Furthermore, the reflection of (020) lattice plane shifted to smaller 2θ angles compared with pristine AlOOH, implying the existence of lattice strain^{31,32}. It demonstrates that the preparation method is conducive to the stripping of the catalyst along the [010] direction. The surface energies of different facets were calculated, and (010) facets had the lowest surface energy, as shown in Supplementary Table 1. The expanded lattice spacings of the as-prepared catalysts can be rationalized in terms of the formation of layered structure AlOOH rather than nanosheets. These are also supported by images (Supplementary Fig. 1) of the other two samples AlOOH-U3, AlOOH-U4.

The FTIR spectra of the catalysts are shown in Fig. 3b. A strong and broad band at ca. 3415 cm⁻¹ in the spectra of all samples are assigned to the stretching vibration of free OH, probably from hydrogen-bonded hydroxyl groups or adsorbed water³⁰. The peak at ca. 1648 cm⁻¹ can be attributed to the bending vibration of surface OH or adsorbed water³³. The peaks at ca. 3099 cm⁻¹ and 1075 cm⁻¹ in the spectra of AlOOH-Ux are attributed to the stretching and bending vibration modes of -OH_{Al-OH}, respectively, further confirming that AlOOH was obtained. However, these two peaks were not observed in the spectrums of AlOx-U1. The band at ca. 738 cm⁻¹ is associated with the vibration mode of AlO₆.

XPS technique was used to analyze the surface state of O elements in the catalysts and the spectra are shown in Fig. 3c. The fitted O1s spectra of AlOOH-U2, AlOOH-U3 and AlOOH-U4 presented three peaks at 529.5–529.8, 530.9–531.1, and 532.3–532.7 eV, attributing to oxygen in lattice structure Al-O-Al (O_L), hydroxyl bound with Al to form Al-OH (-OH_{Al-OH}) or oxygen species (O_{ad}, -OH_{ad}) adsorbed on the surface OH defects and adsorbed water (O_{adH2O}), respectively³³. As a contrast, the deconvolution of the O1s spectrum for AlOx-U1 only gave two peaks at 530.6 eV and 532.1 eV, assigning to the lattice oxygen and surface adsorbed water, which is consistent with the results of FTIR analysis. Compared with AlOx-U1, the Al 2p binding energy (Fig. 3d) for AlOOH-U2, AlOOH-U3 and AlOOH-U4 was lower which was caused by the electron-rich unsaturated Al attributed to OH defects on the surface. In addition, the ratio of O_{adH2O}/O_{Total} of AlOx-U1, AlOOH-U2, AlOOH-U3, and AlOOH-U4 are 39.4, 14.5, 21.6, and 32.9% (Supplementary Table 3), respectively, which is related to the catalytic activity, discussed below.

Catalytic performance. The catalytic performance of the as-prepared catalysts was checked for the hydrogenation of styrene

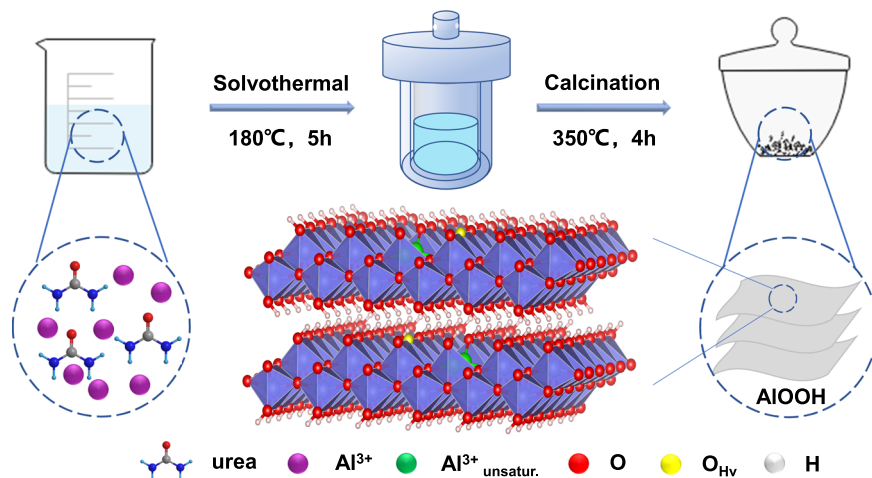


Fig. 1 Catalyst preparation. Schematic process for the fabrication of AIOOH catalyst.

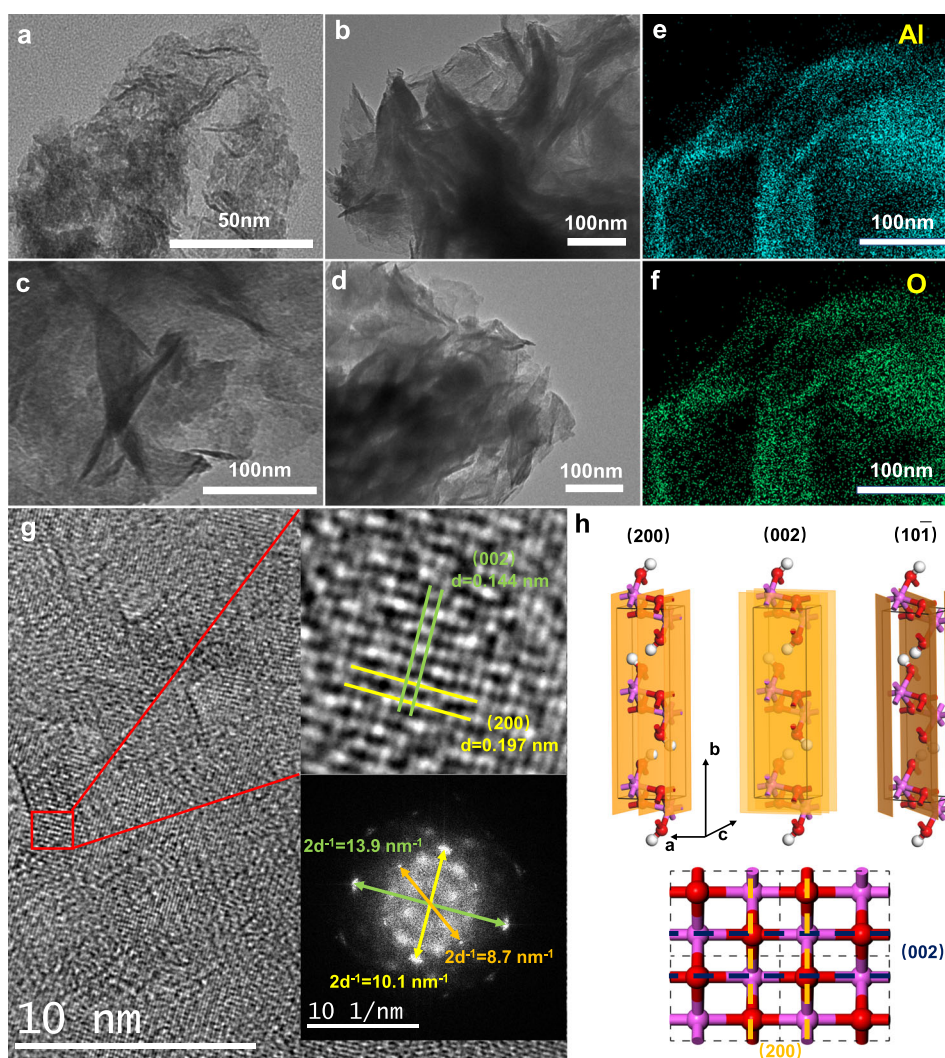


Fig. 2 TEM and HR-TEM images for catalysts. **a** AlO_x-U1. **b** AIOOH-U2. **c** AIOOH-U3. **d** AIOOH-U4. **e** Al and **f** O EDS elemental mapping images of the AIOOH-U2. **g** HR-TEM images of the AIOOH-U2 and the illustration as FFT images. **h** Crystal plane models of (200), (002), (10-1).

to ethylbenzene, as shown in Fig. 3e. The reaction conditions were optimized as shown in Supplementary Table 2. AIOOH-U2 exhibited the best catalytic performance with a complete conversion and >99% selectivity towards ethylbenzene. Despite

the low catalytic activity of AIOOH-U2 observed in the initial 2 h (Supplementary Table 2, entry 5), a satisfying complete hydrogenation of styrene was realized by prolonging the reaction time to 6 h at 80 °C (Supplementary Table 2, entry 7).

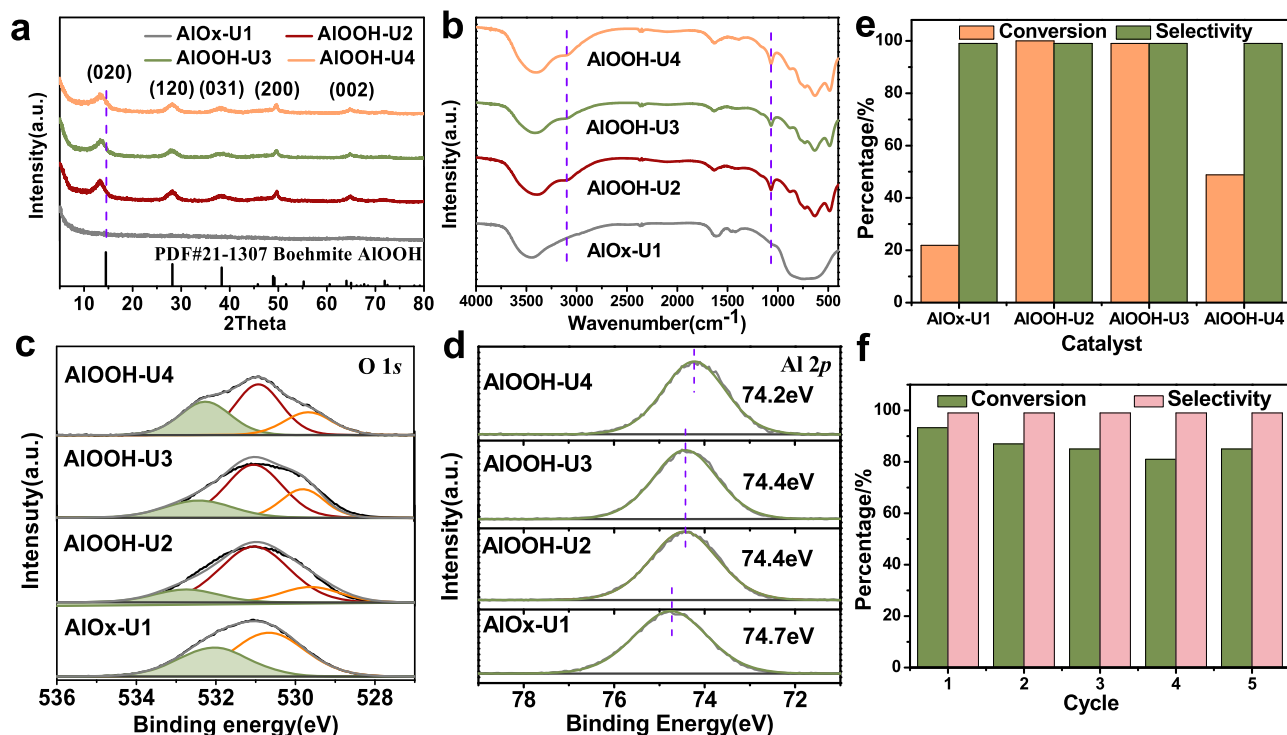


Fig. 3 Characterization and activity of the AlOOH catalyst. **a** XRD **b** FTIR **c** O1s and **d** Al 2p XPS and **e** Reactivity comparison of different catalyst. **f** Catalyst recycling of AlOOH-U2. Catalyst (50 mg), temperature (80 °C), H₂ pressure (2 MPa), time (6 h), styrene (0.5 mmol), THF (2 mL), stirring speed (600 rpm) and n-decane as internal standard.

The reaction process depends upon H₂ pressure and the conversion increases with the increase of H₂ pressure (Supplementary Table 2, entry 10–12).

The reusability of AlOOH-U2 was evaluated under the optimized reaction conditions. The catalysts were recovered by centrifugation and washed with THF several times after reaction, and then dried at 60 °C in a vacuum oven overnight for the next use. The AlOOH-U2 can be used at least 5-times without a considerable decrease in activity and selectivity (Fig. 3f). The almost unchanged phase and layered morphology illustrate that the catalyst AlOOH-U2 is stable during hydrogenation reactions (Supplementary Fig. 2b, d). Furthermore, it should be noted that the activity of AlOOH-U2 after calcination in H₂ flow at 300 °C did not decrease (Table 1, entry 3). The FTIR characteristic peak (ca. 3099 cm⁻¹ and 1075 cm⁻¹) of AlOOH-U2 still existed after calcination, indicating the catalyst was stable under H₂ atmosphere even at 300 °C (Supplementary Fig. 3).

Figure 4a shows the thermogravimetric analysis (TGA) curves for AlOOH-U2. There are two obvious steps of weight loss. The endothermic peak at ca. 97.4 °C is assigned to the loss of physically adsorbed water³⁰. The peak at ca. 446.7 °C is ascribed to the weight loss of hydroxyl groups bonded with Al (-OH_{Al-OH}), *i. e.* the dehydroxylation of AlOOH.

Role of surface defects for hydrogenation. To further confirm the OH defects on the AlOOH surface, electron paramagnetic resonance (EPR) was used to study these catalysts. The EPR results shown in Fig. 4b suggest that there are two kinds of defects in the different chemical environments on the surface of AlOOH³⁴, a OH vacancy (OH_v) and a surface O site (O_{Hv}) created by one H removed from OH. The fitting results of all samples are shown in Supplementary Fig. 4 and a hyperfine coupling from surrounding H species was observed in SysA with an A_H-value of 53.69 MHz (Supplementary Table 4-1). Thus SysA, SysB and SysC could be assigned to Al-OH_v-Al, Al-O_{Hv}-Al

Table 1 The catalytic activity of AlOOH-U2 with different treatment condition.

Entry	Catalyst	Conv./%	Sel./%
1 ^a	AlOOH-U2	0	-
2 ^b	AlOOH-U2	0	-
3 ^c	AlOOH-U2	0	-
4	AlOOH-U2-H ₂ -300 °C	99	>99
5	AlOOH-U2-air-450 °C	17.0	>99
6	AlOOH-U2-Ar-450 °C	100	>99
7 ^d	AlOOH-U2-Ar-450 °C	100	>99

Reaction conditions: Catalyst (50 mg), temperature (80 °C), H₂ pressure (2 MPa), time (6 h), styrene (0.5 mmol), THF (2 mL), stirring speed (600 rpm) and n-decane as internal standard. *a*: H₂O (2 mL) as the solvent. *b*: 5 × 10⁻³ mol L⁻¹ mg_{AlOOH-U2} pyridine as additive. *c*: 5 × 10⁻³ mol L⁻¹ mg_{AlOOH-U2} benzoic acid as additive. *d*: The reaction time was 4 h.

and background signal, respectively. DFT calculation also shows that OH_v and O_{Hv} could form FLPs. A combination of EPR and XPS results revealed that the adsorbed water occupied the defects on the surface of AlOx-U1, AlOOH-U3 and AlOOH-U4, resulting in the decrease in activity. It is easier to construct FLPs with both defects on the catalyst surface.

To clarify the role of surface OH defects, some control experiments were conducted. Based on TGA analysis, the chemical bonds of Al-OH in AlOOH could be broken at ca. 450 °C. The catalyst AlOOH-U2 was calcined in air at 450 °C for 3 h, denoted as AlOOH-U2-air-450 °C. As the FTIR spectra shown in Fig. 4c (green line), two characteristic absorption peaks of AlOOH at ca. 3099 cm⁻¹ and 1075 cm⁻¹ associated with -OH_{Al-OH} disappear, implying that the chemical bonds of Al-OH in AlOOH was broken. The EPR of AlOOH-U2-air-450 °C

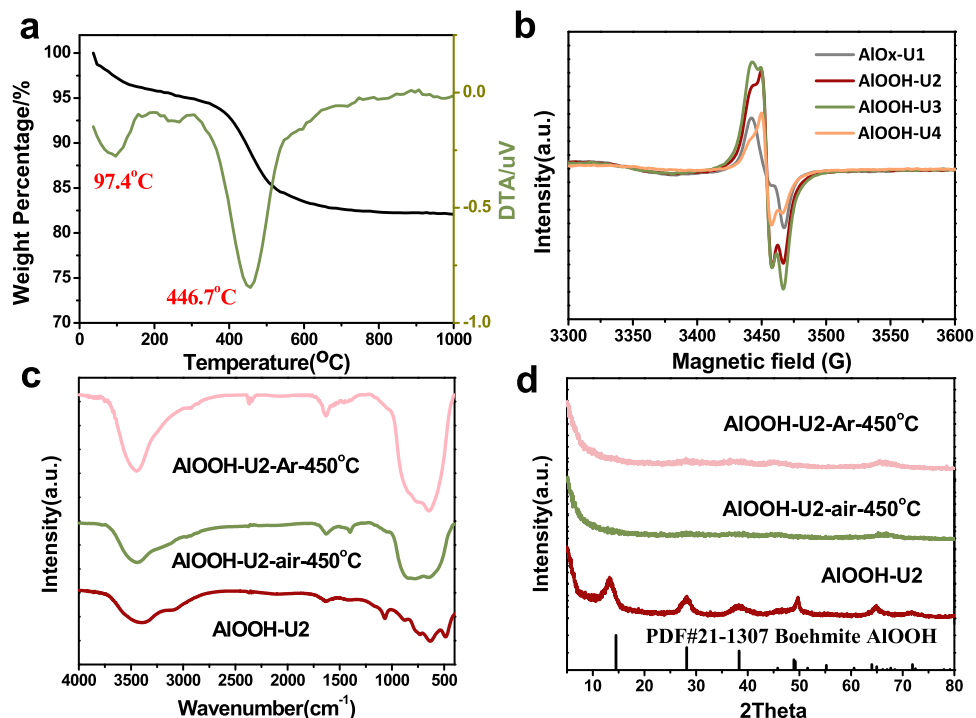


Fig. 4 Characterization of the AlOOH catalyst. **a** TGA analysis of AlOOH-U2 catalyst. **b** EPR spectra of different catalysts synthesized by different urea usage. **c** FTIR spectra and **d** XRD patterns of AlOOH-U2 catalyst with different treatment conditions.

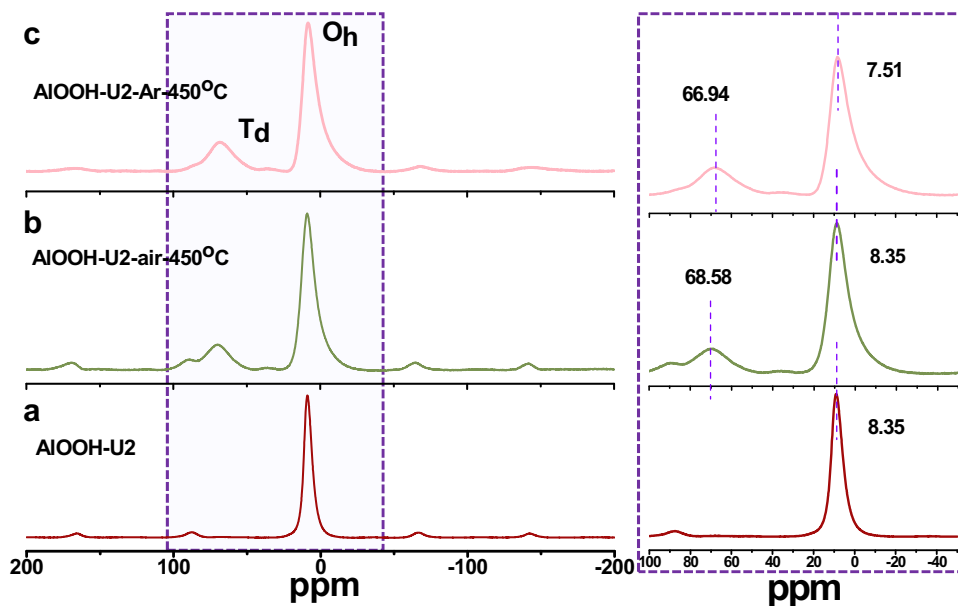


Fig. 5 ²⁷Al solid NMR of AlOOH. Catalyst treated in different conditions. **a** AlOOH-U2. **b** AlOOH-U2-air-450 °C. **c** AlOOH-U2-Ar-450 °C.

(Supplementary Fig. 5) shows a *g* value of 2.003 with only one peak, indicating that the surface FLPs are locked by O after calcination in air. As shown in XRD patterns (Fig. 4d, green line), AlOOH-U2-air-450 °C exhibited an amorphous aluminum oxide structure. However, the layered structure of AlOOH-U2 was preserved for AlOOH-U2-air-450 °C as shown in Supplementary Fig. 2a. As expected, the catalytic activity of AlOOH-U2-air-450 °C was decreased significantly, (Table 1, entry 4). The decreased catalytic activity may be attributed to the disappearance of surface OH defects, which leads to the destruction of FLP sites. For comparison, a perfect FLP surface catalyst was prepared by

treating AlOOH-U2 under Ar atmosphere at 450 °C for 3 h, denoted as AlOOH-U2-Ar-450 °C. The AlOOH-U2-Ar-450 °C also presents an amorphous alumina oxide structure (Fig. 4d, pink line). The FTIR spectra (Fig. 4c, pink line) also show that the stretching and bending vibration modes of -OH_{Al-OH} disappeared. However, a higher field chemical shift was observed in the ²⁷Al NMR of AlOOH-U2-Ar-450 °C compared with AlOOH-U2-air-450 °C (Fig. 5). This was attributed to the electron shielding effects on the Al nucleus caused by abundant OH defects. As expected, the catalytic activity of AlOOH-U2-Ar-450 °C was higher than that of AlOOH-U2. As shown in Table 1, entry 6,

Among the three hydrogen adsorption modes, the net charge of molecular hydrogen in model III was $+0.613 e$, while it was $+0.267 e$ and $+0.218 e$ in the other two modes (Supplementary Fig. 12). The net charge indicates that the Lewis acid site plays a vital role in ALOOH-based FLPs, which was also verified by Hirshfeld population analysis. As shown in Supplementary Table 5–Table 8, the charge on surface O species varied from $-0.826 e$ to $-1.012 e$, however the charge on Al species near defects was $+0.204 e$ in model II and $+1.126 e$ in model III (Supplementary Table 7, 8). Considering with small ion radius and high charge density of Al^{3+} species, its acidity increased sharply when Al coordination decreases. In model I, the removal of one OH group leads to a single electron localized in the defect (Supplementary Fig. 13), which decreased the Lewis acidity of exposed Al as shown in Fig. 6a.

In model III, removal of one H_2O molecule in an appropriate distance from ALOOH (010) surface resulted in no localized single electron on the surface, while it increased the acidity of formed FLPs since Al's orbitals in the defect was not occupied and the electron pair was localized in surface oxygen (O_{Hv}). The twisted Al–O structures near the defect in model III also proved the unoccupied orbitals in the defect and enhanced Lewis acidity, compared to models I and II. The computational studies combined with characterizations have provided obvious evidence for the formation of FLPs on non-reducible oxides and their hydrogen activation ability.

According to our DFT calculations, H_2 adsorbed on ALOOH was readily split into $\text{H}^{\delta+}$ and active H species with charges of $0.144 e$ and $0.015 e$, respectively. One of the $\text{H}^{\delta+}$ bonded to the Lewis base site O_{Hv} to yield $\text{O}-\text{H}^{\delta+}$, and the other active H species was stabilized by surrounding Al atoms. It indicates the mode of H_2 splitting on ALOOH is heterolytic. To test the proposed mechanism, we explored the kinetic isotope effect (KIE) with D_2 in styrene hydrogenation. Before the KIE experiment, we first confirmed that the reaction follows the first-order kinetics with respect to hydrogen pressure (Supplementary Fig. 14a). A primary isotope effect was observed (ratio of reaction rates using H_2 and D_2 , $k_{\text{H}}/k_{\text{D}} = 2.97$) implying the heterolytic dissociation of hydrogen⁴⁰ (Supplementary Fig. 14b). In addition, the GC-MS analysis detected the ethylbenzene with a molecular weight (Mw) 107, indicating the addition of an H atom and a D atom to styrene (Supplementary Fig. 15). These results demonstrate that the H_2 splitting over the ALOOH catalysts occurs via heterolytic mode.

We also notice that the surface hydroxyl groups are not rigidly restrained and may lead to a disordered catalytic surface. To valid the abovementioned mechanism, a disordered surface model was built with ‘heating and quenching’ techniques⁴¹. Since Model III FLP site exhibits the lowest hydrogen dissociation barrier, a similar FLP site is introduced in disorder models. (Supportmental Note 1). The calculated molecular hydrogen activation pathways on the disordered surface show similar reaction energies and barriers to the above ideal surface.

Hydrogenation scope of alkenes and alkynes. The scope of hydrogenation reactions catalyzed by ALOOH-U2 was demonstrated in Table 2. The substrate conversion of 100% was achieved under 80°C for the hydrogenation of *p*-methyl styrene and *p*-chlorostyrene (Table 2, entry 1 and entry 3). For *p*-methoxystyrene, a 92.8% conversion was obtained which was slightly lower than that of *p*-methyl styrene (Table 2, entry 2). The catalytic activity of ALOOH-U2 for 4-*tert*-butylstyrene and *trans*-stilbene was very low due to steric hindrance. The conversion of 4-*tert*-butylstyrene was only 37% at 80°C (Table 2, entry 4). The conversion of *trans*-stilbene was still only 2.3% even by extending the reaction time to 24 h and increasing the temperature to 100°C

(Table 2, entry 6). The lower reactivity of 4-aminostyrene (Table 2, entry 1 and entry 5) could be attributed to the interaction between amino ($-\text{NH}_2$) and $\text{Al}^{3+}_{\text{unsatur}}$. For the hydrogenation of phenylacetylene, styrene and ethylbenzene were yielded. A 100% conversion of phenylacetylene with 97.4% selectivity towards ethylbenzene was obtained under 3.0 MPa H_2 pressure at 80°C (Table 2, entry 7). A complete conversion but only 64.9% olefin selectivity was got for 4-methylphenylacetylene hydrogenation (Table 2, entry 8). For 1-chloro-4-ethynylbenzene and 4-ethynylaniline, the conversions were all over 90% and the selectivity of olefin was slightly higher than that of alkanes (Table 2, entry 9 and 10). For diphenylacetylene, 92.2% conversion was afforded and the selectivity of *cis*-stilbene and *trans*-stilbene was 92.4% and 7.6%, respectively (Table 2, entry 11).

Furthermore, the reactivity of 4-vinylbenzaldehyde was also checked. Only 4-ethylbenzaldehyde was produced, with 54% yield and >99% selectivity. The lower reactivity of 4-vinylbenzaldehyde could be ascribed to the blockage of surface FLP sites on ALOOH by the strong adsorption of $\text{C}=\text{O}$ at the OH vacancy. The DFT calculations further proved the result that the adsorption energies of $\text{C}=\text{O}$ and $\text{C}=\text{C}$ are -1.97 eV and -0.69 eV (Supplementary Fig. 16), respectively.

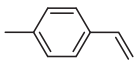
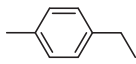
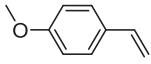
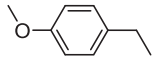
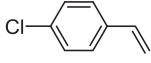
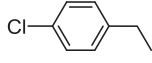
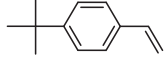
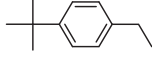
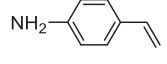
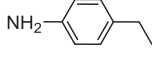
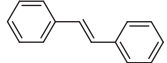
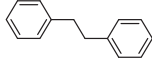
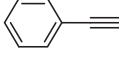
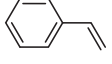

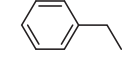
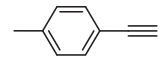
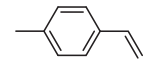

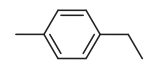
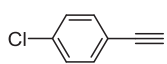
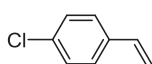
In summary, we constructed a steric independent $\text{O}_{\text{Hv}}/\text{Al}^{3+}_{\text{unsatur}}$ surface FLP sites on non-reducible layered ALOOH for H_2 activation which could efficiently catalyze the hydrogenation of alkenes and alkynes with a wide scope under mild conditions (80°C , 2 MPa). Based on DFT calculations, the H_2 dissociation barrier is as low as 0.16 eV . It is demonstrated that the rich OH defects over ALOOH are the key to generating Lewis base and Lewis acid center. In addition, the layered structure of ALOOH exposes more defects, resulting in a high concentration of $\text{O}_{\text{Hv}}/\text{Al}^{3+}_{\text{unsatur}}$ FLPs, which are conducive to highly efficient hydrogen activation.

Methods

Catalyst preparation. Layered ALOOH were prepared by the solvothermal method. In a typical experiment, 20 mmol $\text{Al}(\text{NO}_3)_3 \cdot 9\text{H}_2\text{O}$ and a certain amount of urea was dissolved in 30 mL deionized water and 30 mL ethylene glycol, respectively. And then the $\text{Al}(\text{NO}_3)_3$ solution was added into the urea solution. After vigorously stirring at room temperature for an hour, the mixture was transferred into a 100 mL Teflon-lined stainless-steel autoclave, followed by a solvothermal treatment at 180°C for 5 h. After being cooled to room temperature, the white translucent gel was separated by centrifugation, washed with deionized water several times until the pH was about 7, and then dried in an oven at 80°C overnight. The final white catalysts were obtained by calcination under an air atmosphere at 350°C for 4 h. The obtained catalysts were denoted as ALOOH-UX, where X refers to the ratio of urea and Al precursor. The catalysts are ground with agate mortar before use.

Catalyst Characterization. The powder X-ray diffraction spectra (Power XRD) measurements were performed on a Rigaku D/max 2500 instrument using Cu K α radiation (50 kV). Transmission electron microscopy (TEM) images were obtained on an HT7700 electron microscope at an acceleration voltage of 120 kV. The element energy dispersive spectroscopy (EDS) mappings were operated at 200 kV on a JEOL-2100F electron microscope. The high-resolution TEM images were obtained at 200 kV on JEM-F200. X-ray photoelectron spectroscopy (XPS) was performed on the Thermo Scientific ESCALab 250Xi using 200 W monochromatic Al K α radiation. The hydrocarbon C1s line at 284.8 eV from adventitious carbon is used for energy referencing. FT-IR spectra of the catalysts with pyridine adsorbed on the catalysts were recorded with a Bruker TENSOR 27 spectrometer. The sample (50 mg) of ALOOH-U2 catalyst was dispersed in a THF solution of pyridine at 80°C and stirred for 8 h. The suspension was centrifuged and washed with THF to remove the physically adsorbed species, and then dried at 60°C for 12 h. The catalysts were blended with KBr for IR characterization. Thermogravimetric analysis (TGA) was done using a Netzsch Germany STA449F3 instrument in N_2 atmosphere at a heating rate of $10^\circ\text{C min}^{-1}$ from room temperature to 1000°C . The products were analyzed quantitatively by a gas chromatograph (Agilent 7890B) equipped with a flame ionization detector (FID). Identification of the products and reactant was done using a GC-MS (Shimadzu QP2010, DB-5MS capillary column) as well as by comparing the retention time with *n*-decane as the internal standard used in GC traces. The EPR data were gained from Bruker EMXplus-9.5/12. ^{27}Al NMR spectra were recorded on a JNM-ECZ600R 600 spectrometer equipped with a 3.2 mm tube diameter. The corresponding resonance frequency and magic angle

Table 2 Scope of AlOOH-U2 for catalytic hydrogenation of alkenes and alkynes ^a.

Entry	Substrate	Product	Temp./°C	Time /h	Pressure /MPa	Conv./%	Sel./%
1 ^b			80	10	2	100	>99
2			80	10	2	92.8	>99
3			80	10	2	100	>99
4			80	10	2	37.0	>99
5			80	10	2	82.9	>99
6			100	24	2	2.3	>99
7			80	24	3	100	2.6 97.4
8			80	24	3	100	64.9 35.1
9 ^b			80	24	3	92.5	80 20
10			80	24	3	92.0	53.8 46.1
11			80	24	3	92.2	92.4 7.6

^a **Reaction conditions:** substrate (0.2 mmol), THF (2 mL), AlOOH-U2 catalyst (50 mg), stirring speed (600 rpm); the substrate conversion and product selectivity were determined by GC with n-decane as internal standard

^b n-Dodecane as internal standard.

spinning rate were 156 MHz and 12 kHz respectively. ^{27}Al NMR measurements were performed without any pretreatment on the samples.

Catalytic activity tests. The reaction was carried out in a Teflon-lined stainless-steel reactor of 16 mL with a magnetic stirrer. In a typical experiment, the desired amount of catalyst, reactant and solvent were added into the reactor. The air in the reactor was replaced with H_2 for 3 times and then the reactor was pressurized with H_2 to a certain pressure. The reactor was put into an air bath at the desired temperature. After a certain reaction time, the autoclave was placed into an ice-water mixture, cooled to room temperature, and a known amount of internal standard n-decane was then added to the reactor. Then the reaction solution was centrifuged to separate the catalyst and the liquid was analyzed by GC analysis. The conversion of reactants and the selectivity of the products were calculated based on the GC data. The reaction experiments of other substrates are the same as those mentioned above.

Computational details. All DFT calculations were performed using QUICKSTEP code³⁵ of CP2K package³⁶. The generalized gradient approximation (GGA) with Perdew-Burke-Ernzerhof (PBE) functional was used to evaluate the exchange and correlation⁴². The wave functions were expanded in a molecularly optimized (MOLOPT) double- ζ Gaussian basis set⁴³ with a cutoff energy of 450 Ry and Goedecker-Teter-Hutter pseudopotentials⁴⁴. The empirical dispersion correction (Grimme D3) within a range of 15 Å was used to correct dispersion effects⁴⁵. All transition states were located with the climbing image NEB method with a force convergence limit of 0.03 eV/Å.

The two-layer p (5 × 4) slab models were based on boehmite crystal structure, and the most stable (010) facet was selected to simulate the catalyst surface. The bottom layer was fixed during geometry optimization to mimic the bulk phase. A 15 Å thick vacuum layer was induced to eliminate the interaction between neighboring slabs.

Data availability

The primary data that support the plots within this paper and other finding of this study are available from the corresponding author on reasonable request.

Received: 14 August 2021; Accepted: 22 March 2022;

Published online: 28 April 2022

References

1. Norskov, J. K. et al. The nature of the active site in heterogeneous metal catalysis. *Chem. Soc. Rev.* **37**, 2163–2171 (2008).
2. Ding, Y. et al. A Heterogeneous Metal-Free Catalyst for Hydrogenation: Lewis Acid-Base Pairs Integrated into a Carbon Lattice. *Angew. Chem. Int. Ed.* **57**, 13800–13804 (2018).
3. Dogra, A. et al. Metal free alkene hydrogenation by B-doped graphitic carbon nitride. *Catal. Sci. Technol.* **10**, 3024–3028 (2020).
4. Su, D. S., Wen, G., Wu, S., Peng, F. & Schlögl, R. Carbocatalysis in Liquid-Phase Reactions. *Angew. Chem. Int. Ed.* **56**, 936–964 (2017).
5. Luo, Z. et al. Transition metal-like carbocatalyst. *Nat. Commun.* **11**, 4091 (2020).
6. Primo, A., Neatu, F., Florea, M., Parvulescu, V. & Garcia, H. Graphenes in the absence of metals as carbocatalysts for selective acetylene hydrogenation and alkene hydrogenation. *Nat. Commun.* **5**, 5291 (2014).
7. Welch, G. C., San Juan, R. R., Masuda, J. D. & Stephan, D. W. Reversible, Metal-Free Hydrogen Activation. *Science* **314**, 1124–1126 (2006).
8. Stephan, D. W. & Erker, G. Frustrated Lewis pairs: metal-free hydrogen activation and more. *Angew. Chem. Int. Ed.* **49**, 46–76 (2010).
9. Eros, G. et al. Expanding the scope of metal-free catalytic hydrogenation through frustrated Lewis pair design. *Angew. Chem. Int. Ed.* **49**, 6559–6563 (2010).
10. Wang, X., Kehr, G., Daniliuc, C. G. & Erker, G. Internal adduct formation of active intramolecular C4-bridged frustrated phosphane/borane Lewis pairs. *J. Am. Chem. Soc.* **136**, 3293–3303 (2014).
11. Stephan, D. W. & Erker, G. Frustrated Lewis pair chemistry: development and perspectives. *Angew. Chem. Int. Ed.* **54**, 6400–6441 (2015).
12. Stephan, D. W. et al. Frustrated Lewis Pairs. *J. Am. Chem. Soc.* **137**, 10018–10032 (2015).
13. Stephan, D. W. et al. The broadening reach of frustrated Lewis pair chemistry. *Science* **354**, aaf7229 (2016).
14. Wang, X. et al. Frustrated Lewis Pairs Accelerating CO_2 Reduction on Oxyhydroxide Photocatalysts with Surface Lattice Hydroxyls as a Solid-State Proton Donor. *Adv. Fun. Mat.* **28**, 1804191 (2018).
15. Lee, H. et al. Formation of frustrated Lewis pairs in Ptx-loaded zeolite NaY. *Angew. Chem. Int. Ed.* **54**, 13080–13084 (2015).
16. Lu, G. et al. Gold catalyzed hydrogenations of small imines and nitriles: enhanced reactivity of Au surface toward H_2 via collaboration with a Lewis base. *Chem. Sci.* **5**, 1082–1090 (2014).
17. Zhang, S. et al. Solid frustrated-Lewis-pair catalysts constructed by regulations on surface defects of porous nanorods of CeO_2 . *Nat. Commun.* **8**, 15266 (2017).
18. Kulbir Kaur, G. et al. Illuminating CO_2 reduction on frustrated Lewis pair surfaces: investigating the role of surface hydroxides and oxygen vacancies on nanocrystalline $\text{In}_2\text{O}_{(3-x)}(\text{OH})_y$. *Phys. Chem. Chem. Phys.* **17**, 14623–14635 (2015).
19. Kulbir Kaur, G. et al. Surface Analogues of Molecular Frustrated Lewis Pairs in Heterogeneous CO_2 Hydrogenation Catalysis. *ACS Catal.* **6**, 5764–5770 (2016).
20. Ghousoub, M., Yadav, S., Ghuman, K. K., Ozin, G. A. & Singh, C. V. Metadynamics-Biased ab Initio Molecular Dynamics Study of Heterogeneous CO_2 Reduction via Surface Frustrated Lewis Pairs. *ACS Catal.* **6**, 7109–7117 (2016).
21. Kulbir Kaur, G. et al. Photoexcited Surface Frustrated Lewis Pairs for Heterogeneous Photocatalytic CO_2 Reduction. *J. Am. Chem. Soc.* **138**, 1206–1214 (2016).
22. Zhao, S. et al. Design of Lewis Pairs via Interface Engineering of Oxide-Metal Composite Catalyst for Water Activation. *J. Phys. Chem. Lett.* **12**, 1443–1452 (2021).
23. Jiang, Y., Xie, Y. & Guo, H. A computational study of energy barriers of structural transformations and hydrogen transfer in boehmite. *RSC Adv.* **8**, 2377–2384 (2018).
24. Zhou, Y. et al. Hydrogenation of methyl propionate over Ru–Pt/AlOOH catalyst: Effect of surface hydroxyl groups on support and solvent. *Catal. Commun.* **11**, 137–141 (2009).
25. Liu, S. et al. Two-dimensional porous γ -AlOOH and γ - Al_2O_3 nanosheets: hydrothermal synthesis, formation mechanism and catalytic performance. *RSC Adv.* **5**, 71728–71734 (2015).
26. Choi, E. et al. Cu/ZnO/AlOOH catalyst for methanol synthesis through CO_2 hydrogenation. *Korean J. Chem. Eng.* **35**, 73–81 (2017).
27. Van Gog, H. First-principles study of dehydration interfaces between diaspore and corundum, gibbsite and boehmite, and boehmite and γ - Al_2O_3 : Energetic stability, interface charge effects, and dehydration defects. *Appl. Sur. Sci.* **541**, 148501 (2021).
28. Sermon, P. A., Bond, G. C. & Web, G. Hydrogenation over boehmite/ γ - Al_2O_3 catalysts. *J. Chem. Soc., Faraday Trans.* **75**, 395–405 (1976).
29. Sassi, M. et al. Surface Hydration and Hydroxyl Configurations of Gibbsite and Boehmite Nanoplates. *J. Phys. Chem. C.* **124**, 5275–5285 (2020).
30. Yan, Z., Xu, Z., Yu, J. & Jaroniec, M. Effect of microstructure and surface hydroxyls on the catalytic activity of Au/AlOOH for formaldehyde removal at room temperature. *J. Colloid. Inter. Sci.* **501**, 164–174 (2017).
31. Zhao, Y. et al. Tuning Oxygen Vacancies in Ultrathin TiO_2 Nanosheets to Boost Photocatalytic Nitrogen Fixation up to 700 nm. *Adv. Mater.* **31**, e1806482 (2019).
32. Iijima, S., Yumura, T. & Liu, Z. One-dimensional nanowires of pseudoboehmite (aluminum oxyhydroxide gamma-AlOOH). *Proc. Natl Acad. Sci.* **113**, 11759–11764 (2016).
33. Xu, Z., Yu, J. & Jaroniec, M. Efficient catalytic removal of formaldehyde at room temperature using AlOOH nanoflakes with deposited Pt. *Appl. Catal. B: Environ.* **163**, 306–312 (2015).
34. Rao, F. et al. Maximizing the Formation of Reactive Oxygen Species for Deep Oxidation of NO via Manipulating the Oxygen-Vacancy Defect Position on $(\text{BiO})_2\text{CO}_3$. *ACS Catal.* **11**, 7735–7749 (2021).
35. VandeVondele, J. et al. Quickstep: fast and accurate density functional calculations using a mixed Gaussian and plane waves approach. *Comput. Phys. Commun.* **167**, 103–128 (2005).
36. Thomas, D. K. et al. CP2K: An electronic structure and molecular dynamics software package-Quickstep: Efficient and accurate electronic structure calculations. *J. Chem. Phys.* **152**, 194103 (2020).
37. Mills, G., Jónsson, H. & Schenter, G. K. Reversible work transition state theory: application to dissociative adsorption of hydrogen. *Surf. Sci.* **324**, 305–337 (1995).
38. Henkelman, G., Uberuaga, B. P. & Jónsson, H. A climbing image nudged elastic band method for finding saddle points and minimum energy paths. *J. Chem. Phys.* **113**, 9901–9904 (2000).
39. Becke, A. D. & Edgecombe, K. E. A simple measure of electron localization in atomic and molecular systems. *J. Chem. Phys.* **92**, 5397 (1990).
40. Liu, P. X. et al. Photochemical route for synthesizing atomically dispersed palladium catalysts. *Science* **352**, 797–801 (2016).
41. Madrid, Jose, Carlos, M. & Kulbir Kaur, G. Disorder in energy materials and strategies to model it. *Adv. Phys. X* **6**, 1848458 (2021).
42. Perdew, J. P., Burke, K. & Ernzerhof, M. Generalized gradient approximation made simple. *Phys. Rev. Lett.* **77**, 3865–3868 (1996).

43. VandeVondele, J. & Hutter, J. Gaussian basis sets for accurate calculations on molecular systems in gas and condensed phases. *J. Chem. Phys.* **127**, 114105 (2007).
44. Hartwigsen, C., Goedecker, S. & Hutter, J. Relativistic separable dual-space Gaussian pseudopotentials from H to Rn. *Phys. Rev. B* **58**, 3641–3662 (1998).
45. Grimme, S., Antony, J., Ehrlich, S. & Krieg, H. A consistent and accurate ab initio parametrization of density functional dispersion correction (DFT-D) for the 94 elements H-Pu. *J. Chem. Phys.* **132**, 154104 (2010).

Acknowledgements

This work was financially supported by the National Key Research and Development Program of China (2017YFA0403103), the National Natural Science Foundation of China (21871277 and 22179132). We thank Professor Jikun Li at the Institute of Chemistry, Chinese Academy of Sciences and Professor Haijun Yang at Tsinghua University for the EPR spectrum discussion. We also thank Professor Jing Xia at the Technical Institute of Physics and Chemistry, Chinese Academy of Sciences and Jing Tai at the Institute of Chemistry, Chinese Academy of Sciences for HR-TEM analysis.

Author contributions

S.L.L. and M.H.D. contributed equally to this work. S.L.L. performed most of the experiments and catalyst characterization. M.H.D. conducted the DFT calculations. Y.X.W. carried out partial control experiments. S.L., Y.X., S.P.L., and J.D. assisted in the catalyst characterization. All authors contributed to discussions and participated in data analysis. S.L.L., M.H.D., H.Z.L., and B.X.H. co-wrote the manuscript with help from all co-authors. H.Z.L. and B.X.H. directed the research.

Competing interests

The authors declare no competing interests.

Additional information

Supplementary information The online version contains supplementary material available at <https://doi.org/10.1038/s41467-022-29970-6>.

Correspondence and requests for materials should be addressed to Huizhen Liu.

Peer review information *Nature Communications* thanks Kyung Byung Yoon, Kulbir Ghuman and the other, anonymous, reviewer for their contribution to the peer review of this work.

Reprints and permission information is available at <http://www.nature.com/reprints>

Publisher's note Springer Nature remains neutral with regard to jurisdictional claims in published maps and institutional affiliations.



Open Access This article is licensed under a Creative Commons Attribution 4.0 International License, which permits use, sharing, adaptation, distribution and reproduction in any medium or format, as long as you give appropriate credit to the original author(s) and the source, provide a link to the Creative Commons license, and indicate if changes were made. The images or other third party material in this article are included in the article's Creative Commons license, unless indicated otherwise in a credit line to the material. If material is not included in the article's Creative Commons license and your intended use is not permitted by statutory regulation or exceeds the permitted use, you will need to obtain permission directly from the copyright holder. To view a copy of this license, visit <http://creativecommons.org/licenses/by/4.0/>.

© The Author(s) 2022